

# Implementation of a T-MOKE setup for transient studies of magnetic materials at the HELIOS XUV photon source

*Project in Physics and Materials Science*

*1FA595, 15 ECTS*

by

PAUL FROEMEL

Supervisor:

JOACHIM RAUSCH,

DR. OLOF KARIS

Co-workers:

DR. JOHAN SÖDERSTRÖM,

DR. MATTIAS SVANQVIST

carried out at

Department of Physics and Astronomy

Molecular and Condensed Matter Physics



UPPSALA  
UNIVERSITET

January 2013

# Contents

<b>1</b>	<b>Abstract</b>	<b>2</b>
<b>2</b>	<b>Motivation</b>	<b>3</b>
<b>3</b>	<b>Introduction to T-MOKE</b>	<b>3</b>
<b>4</b>	<b>Experimental Setup</b>	<b>5</b>
4.1	HELIOS . . . . .	5
4.2	T-MOKE Setup . . . . .	8
<b>5</b>	<b>Experimental Results and Discussion</b>	<b>10</b>
5.1	Multilayer Sample . . . . .	10
5.2	Permalloy . . . . .	12
<b>6</b>	<b>Conclusion</b>	<b>14</b>

# 1 Abstract

The aim of this work was to implement a setup to study transient dynamics in magnetic materials via the transverse magneto-optic Kerr effect (T-MOKE) using ultrashort pulses in the near-infrared and extreme ultraviolet regime supplied by the High-Energy Laser Induced Overtone Source (HELIOS). A T-MOKE setup has been successfully installed at the high-harmonic generation based extreme ultraviolet photon source and first static asymmetry experiments have been conducted on a magnetic multilayer sample and permalloy, proving the setup's capability of monitoring the sample's magnetization with element specificity. Asymmetry factors for Fe and Ni as high as 0.2 and 0.3 have been recorded in good agreement with results published by other groups. Making use of the already existing pump-probe scheme in the near-future, this setup is expected to give insight into the dynamics of (de-)magnetization on a sub-ps timescale.

## 2 Motivation

Information technology is thirsting for storage devices with fast read/write times and high information density. A potential candidate are complex magnetic materials with nanometer structure. Despite its technological importance, a complete understanding of the physical process involved in ultrafast (de-)magnetization remains elusive. Due to the problem's complexity and the experimental difficulty in monitoring the magnetization on ultrafast timescales with element specificity, the role of interaction processes involving photons, electrons, spins and phonons is still debated. One approach to monitor magnetization dynamics element specifically is to take advantage of the transverse magneto-optic Kerr effect at M-shell absorption edges in the extreme ultraviolet (XUV) regime. In this manner, high-harmonic based tabletop XUV photon sources have shown to be capable of resolving differences in demagnetization dynamics as short as 10 fs.<sup>1</sup> In experiments conducted by Mathias et al., energy resolution was achieved by manufacturing the sample in a grating-like structure and diffracting the XUV on a charge coupled device (CCD). However, it is unclear if this grating-like structure might affect the recorded dynamics. Thus, performing similar measurements using a monochromator to achieve the necessary energy resolution could give clearance even though temporal resolution better than 100 fs will already be challenging.

## 3 Introduction to T-MOKE

The **Magneto-Optic Kerr Effect** (MOKE) describes the dependency of light reflected from a magnetic sample on the sample's magnetization. Depending on the direction of the magnetization relative to the plane of incidence one differentiates between polar, longitudinal, and transverse MOKE. The polarization geometry can be seen in Fig. 1. While for polar and longitudinal MOKE the magnetization is in the plane of incidence perpendicular or parallel to the samples surface, in the transverse case the magnetization is perpendicular to the plane of incidence and parallel to the sample surface. Depending on the geometry, the material magnetization affects different properties of the reflected light. In the case of polar and longitudinal MOKE, the sample magnetization leads to a rotation of the reflected light's polarization. In the transverse geometry, one observes a change in the intensity of the reflected light.

This effect can be understood in a intuitive, classical picture if one treats the sample's magnetization as an external magnetic field  $\vec{B}$ . This magnetic field results in the Lorentz force  $\vec{F}_L = q(\vec{E} + \vec{v} \times \vec{B})$  that effectively rotates the material's electric dipole moments  $\vec{d}$  and therefore its polarization density  $\vec{P}$ . In case of polar and longitudinal MOKE, the polarization  $\vec{P}$  rotates out of the plane of incidence resulting in a rotation of the reflected light's polarization. In the magnetization perpendicular to the plane of incidence on the other hand (T-MOKE), the polarization is only rotated within this plane. This leads to a larger component perpendicular to the outgoing electric field and therefore to a higher reflectivity.

In other words, the magnetic moment leads to non-diagonal entries in the permittivity tensor  $\epsilon$  that governs the electric displacement  $\vec{D} = \epsilon_0 \vec{E} + \vec{P} = \epsilon_0 \vec{E} + \chi \epsilon_0 \vec{E} = \epsilon \vec{E}$  and therefore can result in a rotation of the light's polarization or a change in the reflectivity.

Taking advantage of the transverse magneto-optic Kerr effect, one is able to monitor the sample's magnetization by measuring the spectra of the reflected light for opposite magnetization

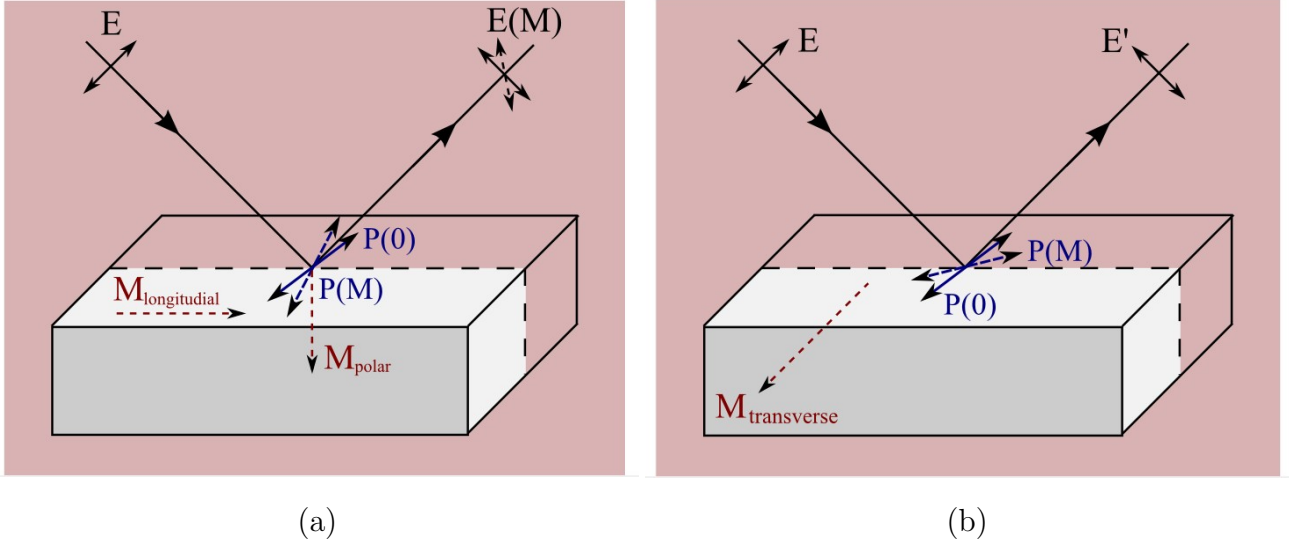


Figure 1: (a) Longitudinal and polar MOKE geometry leading to a rotation of the reflected light's polarization ( $\vec{E}$  and  $\vec{M}$  in plane of incidence) (b) Transverse MOKE geometry, change in the reflected light's intensity induced by transverse magnetization ( $\vec{E}$  in plane of incidence,  $\vec{M}$  perpendicular to plane of incidence).

directions. The so called asymmetry parameter  $A$  defined as

$$A := \frac{I_+ - I_-}{I_+ + I_-} \quad (1)$$

is considered a relative measure for the strength of the sample's magnetization, where  $I_+$  and  $I_-$  are the recorded spectra for the two anti-parallel magnetization directions. Theoretical calculations and experimental results at synchrotron facilities showed a maximum Asymmetry parameter at the quasi-Brewster angle close to  $45^\circ$ .<sup>23</sup> More details on a theoretical model including spin-orbit coupling and exchange splitting of electronic states giving insight into the microscopic light-matter interaction processes can be found in previous work by Erskine et al.<sup>4</sup>

Due to typical M shell absorption edges lying in the XUV regime, using XUV T-MOKE allows one to keep track of the sample's magnetization with element specificity. This is a great advantage when it comes to understanding the underlying physics in transient magnetic dynamics such as ultrafast demagnetization.<sup>1</sup> Moreover, making use of high harmonic generation (HHG) based tabletop XUV photon sources gives access to dynamics on sub-ps timescales.

## 4 Experimental Setup

### 4.1 HELIOS

The HELIOS (High Energy Laser Induced Overtone Source) is a sophisticated laser setup which provides the user with sub-50 fs pulses at high repetition rates in the XUV as well as the near-infrared (NIR) for pump-probe experiments on liquids, gases or solids.

A commercial Ti:Sapphire amplifier (Legend Elite Duo) generates  $<35$  fs, 2.5 mJ, 800 nm pulses at a repetition rate of 5 kHz to drive both the high harmonic generation process and the optical parametric amplifier (OPerA solo). A schematic drawing of the Ti:Sapphire amplifier can be seen in Fig. 2. The main part of the 2.5 mJ output is focused in a noble gas cell to generate ultrashort pulse trains with photon energies from 10 eV up to 100 eV via high harmonic generation. The remaining 0.5 mJ of the Ti:Sapphire amplifier can directly be used as a pump pulse or first drive an optical parametric amplifier (OPerA Solo) to generate pump pulses tunable between 285 nm and 20,000 nm with state-of-the-art pulse duration. Since HHG

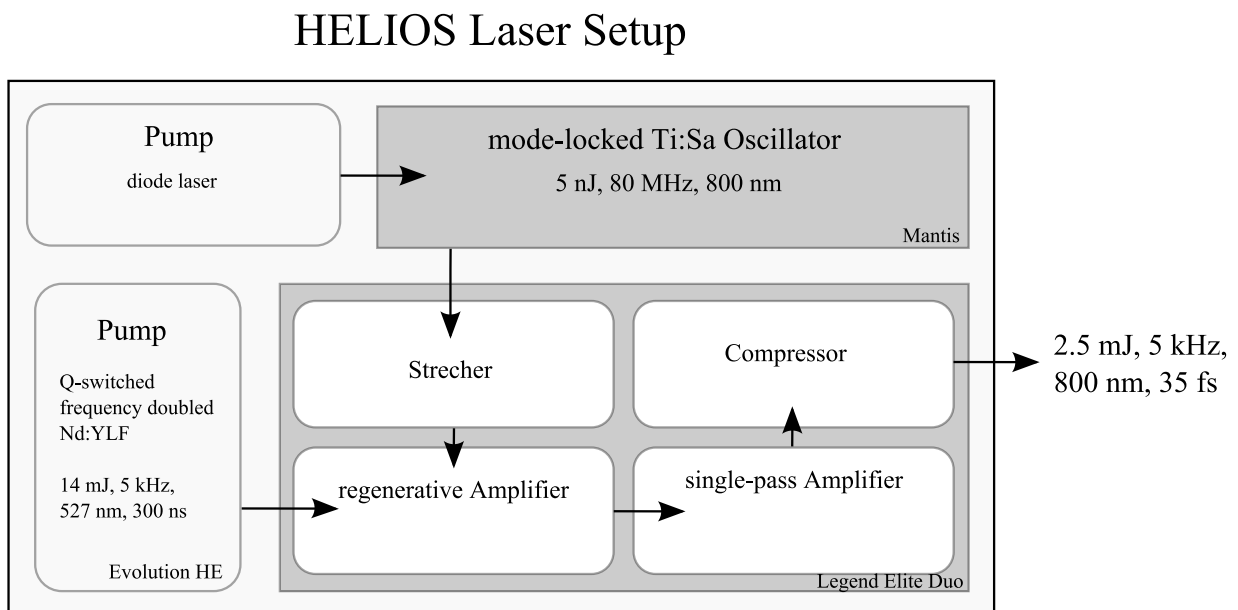


Figure 2: Schematic drawing showing the Ti:Sapphire amplifier layout applied to both drive HHG and OPA.

is the essential process for providing ultrashort XUV pulses, the basics should be recalled at this point. Mcpherson et. al. discovered in 1987 that they were able to generate high overtones of the fundamental wavelength when a strong laser is focused into a noble gas. Furthermore, these high overtones showed a unexpected high number of photons up to several hundred eV which was unprecedented by the known perturbative nonlinear optics. This non-perturbative process can be intuitively understood using the classical so called three-step model. The incident electric field is able to tilt the Coulomb potential strongly enough to induce tunnel ionization (1). After ionization, the free electron is accelerated (2) in the electric field. When the electric

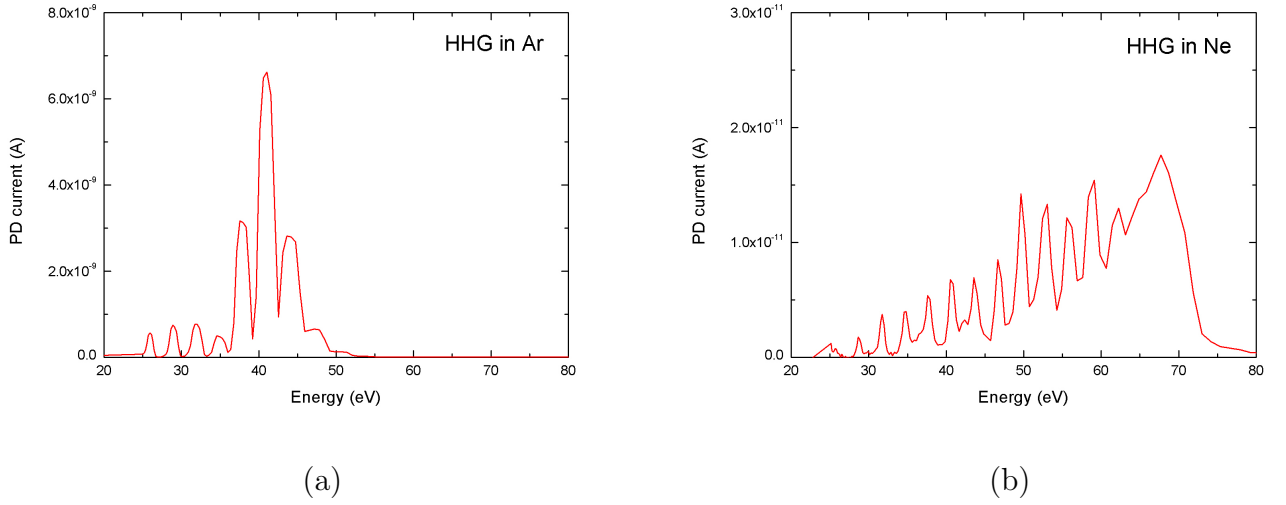


Figure 3: Spectra of high harmonics from (a) Argon and (b) Neon, recorded on a photodiode after the collimation chamber. The energy scale is calibrated using the zero order angle and the cut-off at 72.5 eV due to an Aluminum filter implemented in the monochromator.

field changes its' sign, the electron is accelerated back and recombines with its' parental atom. During this recombination process (3) the excess kinetic energy gained due to acceleration is relieved as a high energy photon. A simple cut-off rule for the maximum achievable photon energy

$$E_{max} = I_P + 3.17 \cdot U_P \approx I_L \lambda_L^2 \quad (2)$$

can be retrieved using a single atom model where  $U_P$  is the free electron's average energy in the strong electric field (ponderomotive potential),  $I_P$  the ionization potential,  $I_L$  and  $\lambda_L$  the laser's intensity and wavelength. Due to the inversion symmetry of the monoatomic noble gas, only odd higher harmonics are generated. Two typical spectra from HHG in Argon and Neon were recorded at HELIOS and are shown in Fig. 3. As can be seen here, a lighter noble gas is capable of producing higher photon energies due to its' greater ionization potential, but comes in general with the disadvantage of lower conversion efficiency. It should be noted that the cut-off in the Neon spectra is due absorption in an Aluminum filter which is placed in the monochromator to protect the exit slit from the residual NIR pulse. The energy resolution in the spectra is accomplished by making use of a single grating monochromator. The monochromator has to achieve good energy resolution while maintaining a good temporal XUV profile capable of conducting sub-ps pump-probe experiments. Since grating geometries used in common high energy resolution monochromators lead to a increase of the XUV pulse duration to several hundred femtoseconds, a more sophisticated design has to be used. The classical method is to use a dual-grating geometry, where the second grating compensates for the chirp introduced by the first grating. However, this geometry is rather complex in its design, requires very precise alignment and comes with relatively poor total transmission. A much higher optical throughput can be achieved by using only one grating in an off-plane geometry.<sup>5</sup> In this case, the grooves are aligned parallel to the plane of incidence and the different wavelengths are diffracted on a cone around the axis through the grating center parallel to the grooves. In the design employed

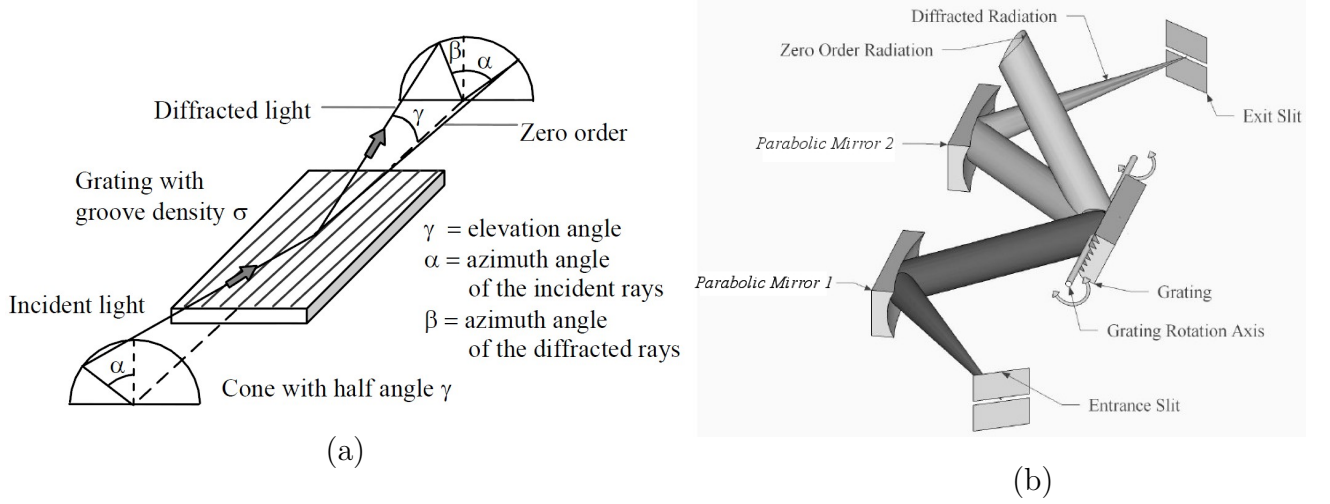


Figure 4: (a) Schematic drawing showing the off-plane grating where the azimuth angle  $\beta$  is dependent on the diffracted light's wavelength. (b) Off-plane monochromator design including collimating mirror, off-plane grating, focusing mirror, and exit slit. Image source: Frassetto et al. (2005).<sup>5</sup>

at HELIOS, a parabolic mirror first collimates the XUV coming from the HHG cell and sends the beam on the off-plane grating. The diffracted beam is then focused on a exit slit to provide the necessary energy resolution. By rotating the off-plane grating the HHG spectrum can be scanned or one specific wavelength can be selected. With the azimuth angles  $\alpha$  and  $\beta$  and the altitude angle  $\gamma$  defined as indicated in Fig. 4a, the grating equation becomes

$$\sin \gamma (\sin \alpha + \sin \beta) = m \lambda \sigma, \quad (3)$$

where  $m$  is the diffraction order,  $\lambda$  the diffracted wavelength and  $\sigma$  the groove density. In the simple case of two parallel aligned parabolic mirrors before and after the off-plane grating ( $\alpha = \beta$ ) this results in

$$2 \sin \gamma \sin \alpha = m \lambda \sigma. \quad (4)$$

At HELIOS, the elevation angle is kept constant at  $\gamma = 3.5^\circ$  at all times. Since the gratings is only operated in blazing mode for one specific wavelength, the grating efficiency varies strongly with the selected energy. In addition, a compromise between high energy resolution and high optical throughput has to be found by selecting the proper groove density and exit slit width. Therefore, the monochromator is equipped with a motorized stage containing four interchangeable gratings. A set of two gratings are optimized for energies around 27 eV with either high energy resolution or high optical throughput while another set of two are optimized for higher photon energies. More details on the HELIOS setup including the off-plane grating monochromator can be found in previous work by S. Plogmaker.<sup>6</sup>

A schematic drawing of the complete planned beamline can be seen in Fig. 5. In the final stage the monochromator will be combined with two end stations consisting of a magnetic bottle for experiments on liquids and a solid state system. For the work presented in this report, the end stations are replaced with a T-MOKE (transverse Magnetic optical Kerr effect) chamber which is described in the next section.

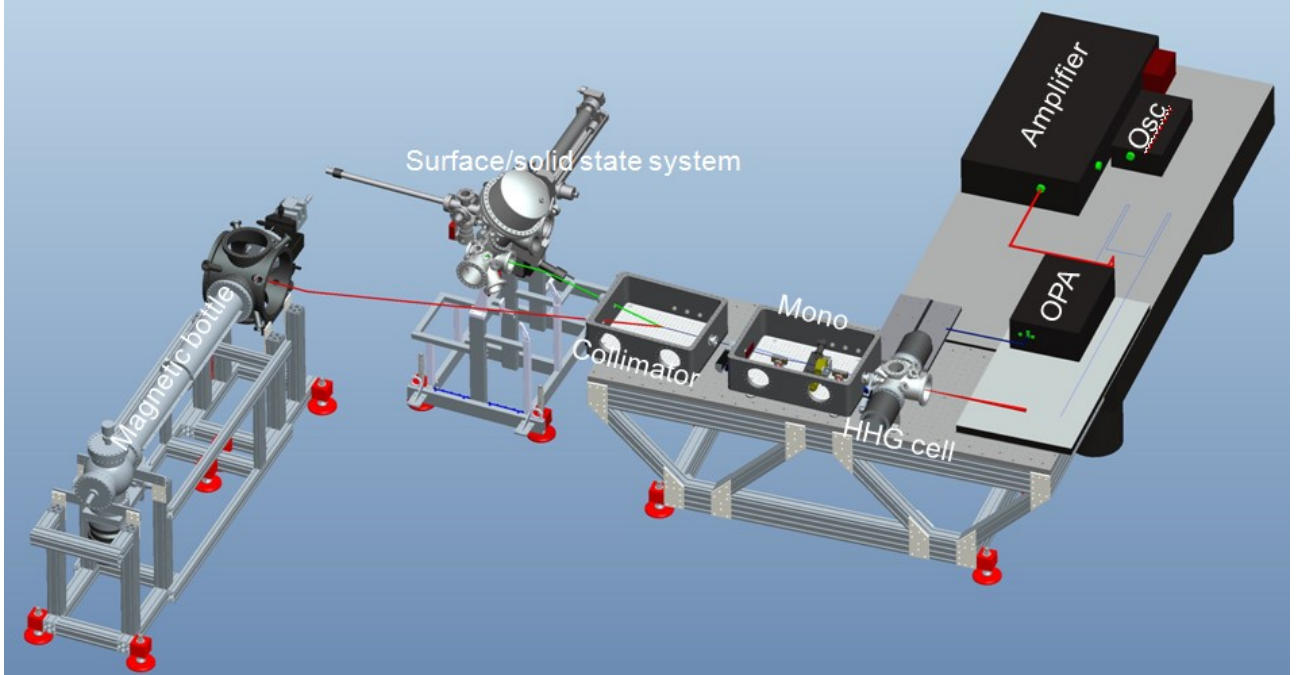
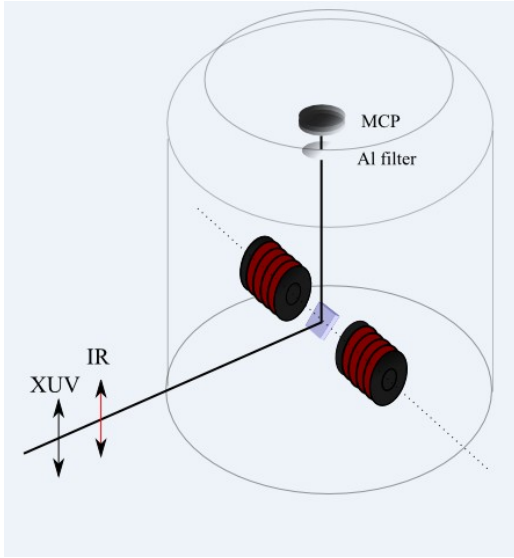


Figure 5: HELIOS setup showing optical table with Ti:Sa Oscillator (Mantis), two stage chirped pulse amplifier (Legend), 2 mJ of amplifier output are focused into noble gas cell to drive HHG while the remaining 0.5 mJ are either directly used as a pump pulse or after frequency conversion via optical parametric amplification (OPerA Solo). The HHG is followed by an off-angle grating monochromator and a re-collimation chamber. The drawing is showing a magnetic bottle experiment for experiments on liquids and a solid state system on the second beam line which has been replaced by the T-MOKE chamber for this work.

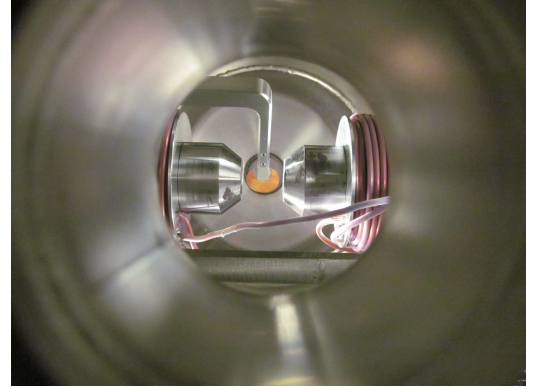
## 4.2 T-MOKE Setup

A ultra high vacuum (UHV) chamber which has previously been employed for NIR longitudinal MOKE (L-MOKE) experiments has been modified, further equipped and connected to the HELIOS beamline to conduct T-MOKE experiments (see Fig. 6). During measurements, pressures lower than  $10^{-7}$  mbar could be easily achieved in the MOKE chamber. In order to achieve a maximum asymmetry factor, a near- $45^\circ$  reflection geometry has been chosen. The XUV light coming from the collimation chamber is reflected with p-polarization from the sample's surface. Two magnets are set to change the sample's magnetization perpendicular to the plane of incidence. These magnets are driven by a 45 A power supply and are estimated to give magnetic field strengths of the order of 50 Oe, enough to switch the sample's magnetization. A U-shape aluminum sample holder has been manufactured to center the sample in the beamline

and enable to rotate the sample around the axis through the sample's center and perpendicular to the plane of incidence. Furthermore, a micro channel plate (MCP) detector has been attached to the XYZ-manipulator in the reflected beam to enable optimal flexibility. A total voltage of 1700 V is applied over the two microchannel plates to enhance the signal by a factor of  $10^6$ . The MCP detector is mounted inside a housing with a opening towards the sample to shield from scattered light and charged particles. To protect the MCP plates from the NIR pump pulse reflected directly from the sample, a 200 nm thick aluminum filter is covering the opening towards the sample. Furthermore, the aluminum filter is tilted by  $\approx 10^\circ$  to prevent NIR back-reflection to the sample.



(a)



(b)

Figure 6: (a) Schematic drawing of the T-MOKE chamber. Ultrashort XUV and IR pulse are reflected at  $45^\circ$  from sample surface for maximum asymmetry factor. Reflected XUV photons are measured on a MCP detector after separating the IR pulse by an 200 nm thick, tilted Aluminum filter. Two magnets are employed to switch the sample magnetization between the measurements. (b) Photograph of Cu plate with florescent powder in sample holder which has been used for optimal XUV alignment.

For the static asymmetry measurements, the sample is magnetized first in one direction by driving the magnets with a current in one direction. Afterwards, the HHG spectra " $I_+$ " is scanned by rotating the off-plane grating while measuring the XUV photon flux on the MCP. The magnets are driven in the opposite direction to switch the sample's polarization before the reflected XUV spectra " $I_-$ " is recorded again. By applying equation 1, the asymmetry factor can be retrieved and the sample's magnetization can be monitored. To achieve temporal resolution in future experiments, part of the NIR pulse are split before the HHG cell and recombined with the XUV in the collimation chamber for a colinear pump-probe scheme. Moreover, an optical parametric amplifier (OPerA Solo) with state-of-the-art temporal resolution allows to access pump pulse wavelengths in the broad range of 285 – 20,000 nm.

## 5 Experimental Results and Discussion

### 5.1 Multilayer Sample

The first sample studied was a magnetic multilayer structure consisting of alternating magnetic and nonmagnetic heusler alloys  $\text{Co}_2\text{MnGe}$  and  $\text{Rh}_2\text{CuSn}$ . This double layer with a thickness of 3.6 nm is repeated 13 times and protected with a 3 nm thick  $\text{Rh}_2\text{CuSn}$  cap. This multilayer structure was originally grown for GMR measurements and therefore comes with additional layers consisting of  $\text{Co}_{70}\text{Fe}_{30}$ , Ru, and Ta. However, these layers are not penetrated by the XUV due to its short attenuation length.

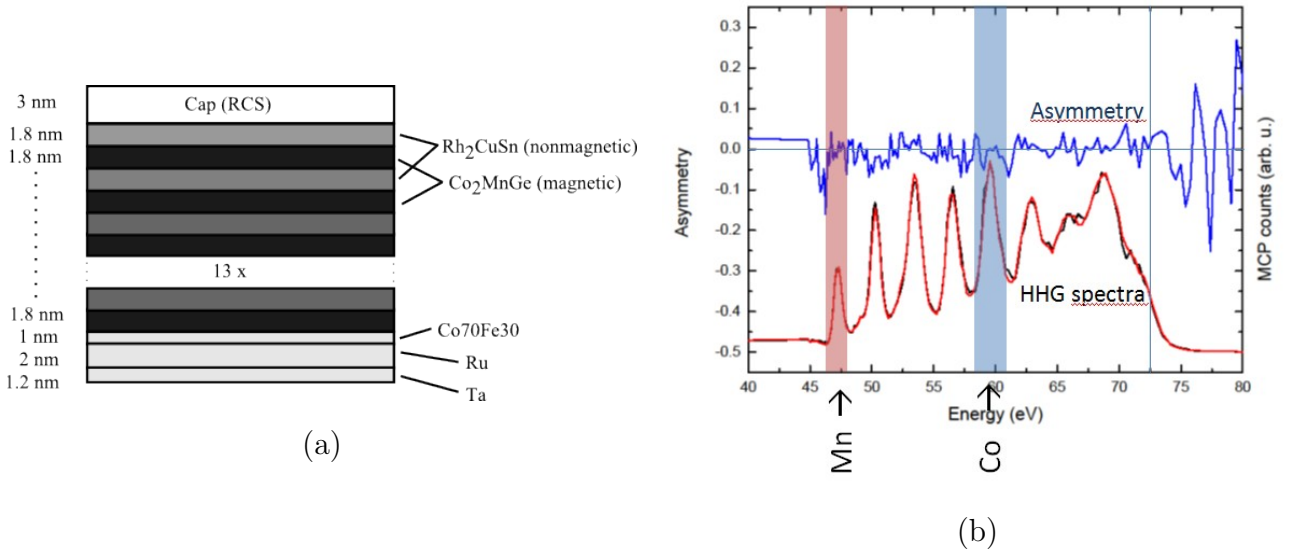
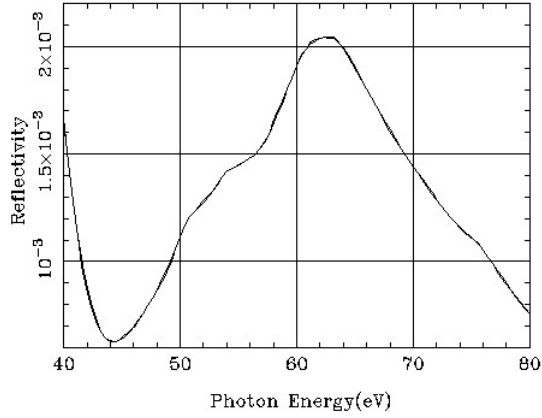


Figure 7: (a) Magnetic multilayer sample containing 13 alternating layers of the magnetic heusler  $\text{Co}_2\text{MnGe}$  and the nonmagnetic heusler  $\text{Rh}_2\text{CuSn}$  (b) Static asymmetry measurement on magnetic multilayer sample. Inset showing the two recorded HHG spectra  $I_+$  and  $I_-$  from which the asymmetry factor is calculated. Peaks below 46 eV and above 72.5 eV are noise due to low HHG signal. No clear sign of asymmetry could be found at the expected HHG peaks. This is most likely due to absorption in the thick nonmagnetic cap layer.

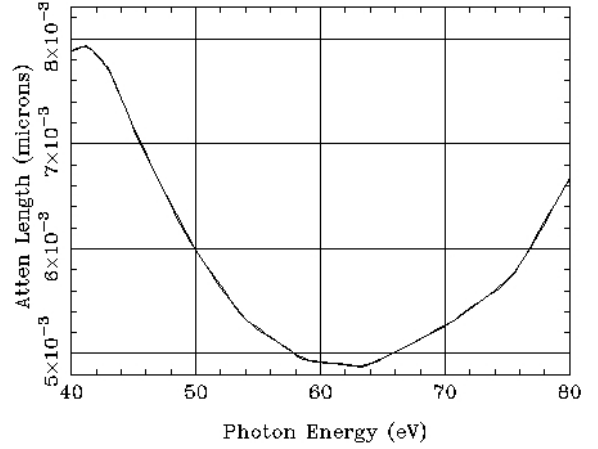
In this sample it was planned to look at the M shell absorption edges of Mn and Co at 47.2 eV and 58.9 eV. The results of the first asymmetry measurements can be seen in Fig. 7. The high-order harmonics were generated in Neon to reach higher conversion efficiency at the desired photon energy. However, no clear sign of asymmetry could be seen in this data. It is expected that this is a result of the relatively thick nonmagnetic cap layer (4.8 nm in total) and the RCS attenuation length being as short as 5 nm at the desired energies (see Fig. 8b). Under an angle of incidence of  $45^\circ$  and exponential decay, only a total of less than 26 % of the incident XUV photons would be able to reach the first magnetic layer. A small portion of these photons ( $< 0.5\%$  @ 58.9 eV) is reflected at the magnetic layer and propagates again through the cap layer where another 74% are absorbed. Therefore, the contribution of the photons carrying the asymmetry signal is  $< 10\%$  of the total reflected XUV which results in a change in the asymmetry lower than the background noise recorded in Fig. 7b. In other words, the dependency of this sample's reflectivity on its magnetic orientation was lower than the

Rh<sub>2</sub>CuSn/Co<sub>2</sub>MnGe d=3.6nm s=0.nm N=13 at 45.deg, P=-1.



(a)

Rh<sub>2</sub>CuSn Density=12.41, Angle=45.deg



(b)

Figure 8: (a) Reflectivity of a multilayer structure consisting of 13 pairs of 1.8 nm thick layers of Rh<sub>2</sub>CuSn and Co<sub>2</sub>MnGe (b) Attenuation length vs photon energy for Rh<sub>2</sub>CuSn at an angle of 45° calculated with database from Center for X-ray Optics (CXRO) at Lawrence Berkeley National Lab (LBNL).<sup>7</sup>

fluctuation in the recorded XUV flux. Therefore, no asymmetry signal could be retrieved from the conducted reflectivity measurements. A calculation of the multilayer sample's reflectivity can be seen in Fig.8a. The measurements on this sample show that the XUVs small penetration depth can become an issue when it comes to studying complex multilayer structures. These challenges could be addressed by improving the signal-to-noise-ratio, e.g. by increasing the integration time and reducing the samples cap layer.

Nevertheless, XUV T-MOKE is a surface sensitive measure due to its intrinsically short attenuation lengths (one is always interested in the reflectivity at the materials absorption edges) and great care has to be taken when studying the magnetic moments of layers distant from the sample's surface.

## 5.2 Permalloy

The second sample that was studied is the magnetic alloy  $\text{Ni}_{0.8}\text{Fe}_{0.2}$ , also termed permalloy. This sample has already been studied with T-MOKE by Mathias et al. in a pioneering but also highly disputed work on ultrafast demagnetization with a HHG based XUV photon source. Instead of using a monochromator, the energy resolution was achieved in their experiment by manufacturing the sample in a grating-like structure and diffracting the HHG on a CCD camera. This has the advantage of avoiding the monochromator's limited temporal resolution. However, manufacturing the sample in a grating-like fashion is challenging and comes in general with considerably lower grating efficiency. Permalloy is an ideal sample for first pump-probe studies to prove the setup's capability, since the retrieved asymmetry factors can be compared with already existing data. In addition, the comparison could give insight into the effect of the sample's grating structure on the results.

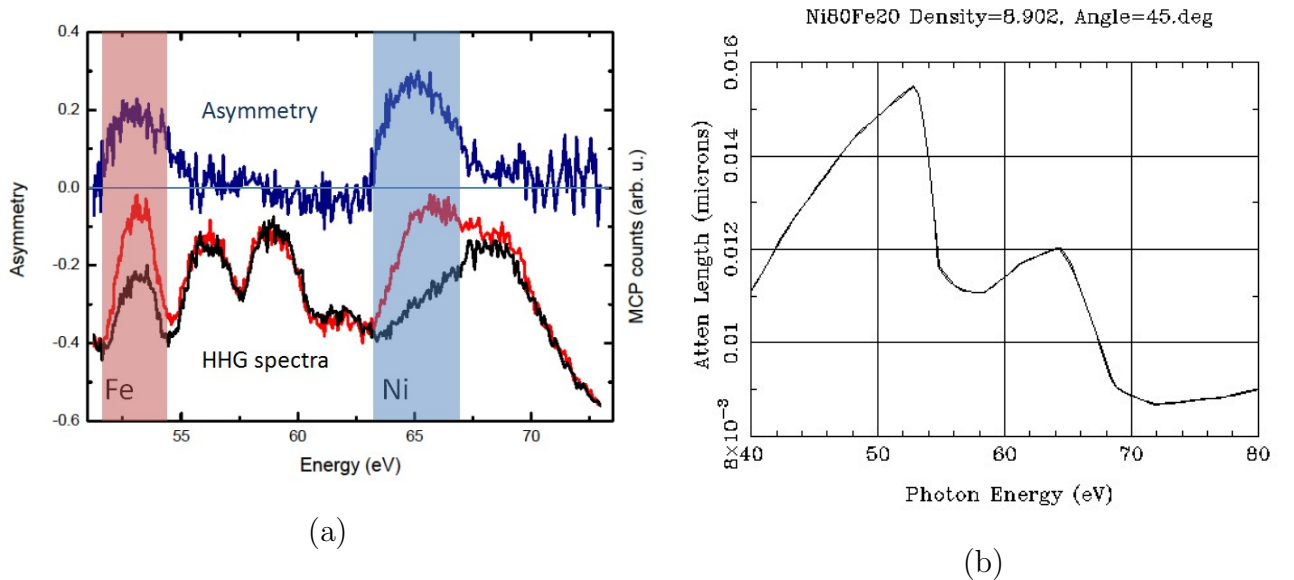


Figure 9: (a) Static asymmetry measurement on permalloy. Inset showing the two recorded HHG spectra  $I_+$  and  $I_-$  from which the asymmetry factor is calculated. Strong asymmetry peaks of up to 0.3 are measured at the Fe and Ni absorption edges (b) Permalloy attenuation length vs photon energy at an angle of  $45^\circ$  calculated with database from Center for X-ray Optics (CXRO) at Lawrence Berkeley National Lab (LBNL).<sup>7</sup>

The studied permalloy sample is 100 nm thick and comes without a cap layer. When possible, it has been kept in a  $N_2$  atmosphere to avoid oxidation before it has been placed into the T-MOKE chamber. The M shell absorption edges in permalloy are at 52.7 eV (Fe) and 66.2 eV (Ni). Therefore, the HHG is once again performed in Neon to reach the necessary photon energies. As can be seen in Fig. 9b, attenuation lengths in permalloy are in the order of 10 – 15 nm at the desired photon energies. Therefore, the penetration depth in permalloy is much larger than in the multilayer sample. Furthermore, the lack of a cap layer on top of permalloy avoids undesired absorption and reflection in nonmagnetic material which would be resulting in a weaker asymmetry signal. The results in Fig. 9 show asymmetry factors of up to 0.2 at the Fe absorption edge and up to 0.3 for Ni. The asymmetry function is in good

agreement with results published by Mathias et al. in 2012 on a grating-like permalloy sample. This proves the built setup's capability of monitoring magnetization with element specificity. Of great scientific interest would be to get record the dynamics of this asymmetry, especially when it comes to comparing with data retrieved from a grating-like permalloy structure to clear the question on the gratings effect on the measured results. Unfortunately, making use of the already existing pump-probe scheme to study the magnetization with temporal resolution was beyond the scope for this work. Nevertheless, time-resolved experiments will be conducted in the future with this setup, hopefully leading to better a understanding of the ultrafast processes involved in (de-)magnetization.

## 6 Conclusion

In summary, a T-MOKE setup has been successfully implemented at the HHG-based XUV photon source HELIOS. First experiments conducted on a magnetic multilayer sample stress that XUV T-MOKE is a surface sensitive technique and great care has to be taken when it comes to designing and selecting complex materials for this experiment.

On the other hand, static measurements in permalloy showed that the constructed setup is capable of monitoring the sample's magnetization with element specificity by looking at asymmetry peaks at the studied element's M shell absorption edges. Asymmetry factors of up to 0.2 for Fe and up to 0.3 for Ni were recorded and are in good agreement with results published by Mathias et al. in 2012.

The next steps include improving the XUV signal by phasemodulation of the IR beam to reach higher conversion efficiency in the HHG process. Furthermore, using a grating and a detector with spatial resolution after the sample instead of scanning with the monochromator could both increase the photon flux and the possible temporal resolution. Employing the already existing NIR pump - XUV probe scheme in the near future is expected to give insight into the dynamics of (de-)magnetization on a sub-ps timescale.

---

## References

- [1] Stefan Mathias et al. Probing the timescale of the exchange interaction in a ferromagnetic alloy. *PNAS*, 109(13):4792–4797, 2012.
- [2] H. Höchst, D. Rioux, D. Zhao, and D. L. Huber. Magnetic linear dichroism effects in reflection spectroscopy: A case study at the fe m<sub>2,3</sub> edge. *J. Appl. Phys.*, 81:7584, 1997.
- [3] M. Sacchi, G. Panaccione, J. Vogel, A. Mirone, and G. van der Laan. Magnetic dichroism in reflectivity and photoemission using linearly polarized light: 3 p core level of ni(110). *Phys. Rev. B*, 58:3750, 1998.
- [4] J. L. Erskine and E. A. Stern. Magneto-optic kerr effects in gadolinium. *Phys. Rev. B*, 8:1239, 1973.
- [5] F. Frassetto, S. Bonora, O. Villoresi, and L. Poletto. Design and characterization of the xuv monochromator for ultrashort pulses at the artemis facility. *Proc. of SPIE*, 7077:707713, 2008.
- [6] Stefan Plogmaker. Techniques and application of electron spectroscopy based on novel x-ray sources. *Digital Comprehensive Summaries of Uppsala Dissertations from Faculty of Science and Technology 903*, 2012.
- [7] Lawrence Berkeley National Laboratory The Center for X-ray Optics. Database for x-ray constants. [http://henke.lbl.gov/optical\\_constants/](http://henke.lbl.gov/optical_constants/), 2013.